ISSN 1674-1056
http://cpb.iphy.ac.cn
http://iopscience.iop.org/cpb
中国物理 B
Chinese Physics
中国物理
Chinese Physics B

Tunable graphene-based mid-infrared band-pass planar filter and its application

Somayyeh Asgari, Hossein Rajabloo, Nosrat Granpayeh, Homayoon Oraizi

Citation: Chin. Phys. B . 2018, 27(8): 084212. **doi:** 10.1088/1674-1056/27/8/084212

Journal homepage: http://cpb.iphy.ac.cn; http://iopscience.iop.org/cpb

What follows is a list of articles you may be interested in

Reduced graphene oxide as saturable absorbers for erbium-doped passively mode-locked fiber laser

Zhen-Dong Chen(陈振东), Yong-Gang Wang(王勇刚), Lu Li(李 璐), Rui-Dong Lv(吕瑞东), Liang-Lei Wei(韦良雷), Si-Cong Liu(刘思聪), Jiang Wang(王 江), Xi Wang(王茜)

Chin. Phys. B . 2018, 27(8): 084206. **doi:** 10.1088/1674-1056/27/8/084206

Ultra-broadband polarization splitter based on graphene layer-filled dual-core photonic crystal fiber

Hui Zou(邹辉), Hui Xiong(熊慧), Yun-Shan Zhang(张云山), Yong Ma(马勇), Jia-Jin Zheng(郑加金)

Chin. Phys. B . 2017, 26(12): 124216. **doi:** 10.1088/1674-1056/26/12/124216

Asymmetrical plasmon reflections in tapered graphene ribbons with wrinkle edges

Cui Yang(杨翠), Runkun Chen(陈闰堃), Yuping Jia(贾玉萍), Liwei Guo(郭丽伟), Jianing Chen(陈佳宁)

Chin. Phys. B . 2017, 26(7): 074220. **doi:** 10.1088/1674-1056/26/7/074220

Solar-blind ultraviolet band-pass filter based on metal-dielectric multilayer structures

Wang Tian-Jiao, Xu Wei-Zong, Lu Hai, Ren Fang-Fang, Chen Dun-Jun, Zhang Rong, Zheng You-Dou

Chin. Phys. B . 2014, 23(7): 074201. **doi:** 10.1088/1674-1056/23/7/074201

Detection of the spatiotemporal field of a single-shot terahertz pulse based on spectral holography

Wang Xiao-Lei, Fei Yang, Li Lu-Jie, Wang Qiang, Zhu Zhu-Qing

Chin. Phys. B . 2014, 23(6): 064202. **doi:** 10.1088/1674-1056/23/6/064202

Tunable graphene-based mid-infrared band-pass planar filter and its application

Somayyeh Asgari[1], Hossein Rajabloo[2], Nosrat Granpayeh[1,†], and Homayoon Oraizi[3]

[1] *Center of Excellence in Electromagnetics, Optical Communication Laboratory, Faculty of Electrical Engineering, K N Toosi University of Technology, Tehran, Iran*

[2] *Young Researchers and Elite Club, Azadshahr Branch, Islamic Azad University, Azadshahr, Iran*

[3] *Department of Electrical Engineering, Iran University of Science and Technology, Tehran, Iran*

(Received 7 February 2018; revised manuscript received 10 April 2018; published online 10 July 2018)

We have designed and proposed the edge modes supported by graphene ribbons and the planar band-pass filter consisting of graphene ribbons coupled to a graphene ring resonator by using the finite-difference time-domain numerical method. Simulation results show that the edge modes improve the electromagnetic coupling between devices. This structure works as a novel, tunable mid-infrared band-pass filter. Our studies will benefit the fabrication of planar, ultra-compact nano-scale devices in the mid-infrared region. A power splitter consisting of two output ribbons that is useful in photonic integrated devices and circuits is also designed and simulated. These devices are useful for designing ultra-compact planar devices in photonic integrated circuits.

Keywords: band-pass filter, graphene, surface plasmons, power splitter

PACS: 42.79.Ci, 61.48.Gh, 71.45.Gm, 42.79.Fm **DOI:** 10.1088/1674-1056/27/8/084212

1. Introduction

Surface plasmon polaritons (SPPs) are electromagnetic surface waves coupled to oscillations of free electrons in metals; theey propagate along metal-dielectric interfaces,[1] and guide lightwaves in subwavelength metallic devices. Recently, different kinds of optical devices based on SPPs have been proposed and analyzed.[2–5] However, it is difficult to vary and control the permittivity functions of noble metals; hence, their abilities are limited in plasmonic devices.

Graphene, an optical material with one thin layer of carbon atom, can be a wonderful material because of its unique and remarkable optical features such as low losses, long propagation length, extreme confinement of the lightwave, and tunable conductivity, which is the most important advantage of graphene compared to the noble metals.[6,7] Graphene utilized as a novel material for generating new nano-scale optical devices.[8,9]

Recently, a wide variety of researches have promoted the development of various types of graphene-based plasmonic devices such as optical waveguides,[10] nano antennas,[11] switches,[12,13] modulators,[14,15] filters,[16,17] metamaterials,[18] metasurfaces,[19] and gratings.[20] Graphene supports two kinds of surface plasmon polariton (SPP) modes: the waveguide modes that the electromagnetic field is confined in along the whole area of the sheet, and the edge modes that the field is confined on the rims of the ribbon.[21–25]

In this paper, we have proposed and analyzed the performance of a novel planar graphene based band-pass filter composed of graphene input/output ribbons and a graphene ring resonator between them. As an application of our proposed planar filter, a power splitter is designed and analyzed. We have analyzed and simulated the performance of the devices by using the three-dimensional finite-difference time-domain (3D-FDTD) numerical method to excite the edge mode.[26,27] In Ref. [26], a planar band stop filter, which is a filter that passes most frequencies unaltered, but attenuates a specific frequency range, has been designed and proposed. In this paper, a planar band pass filter, which is a filter that passes frequencies within a certain range and rejects frequencies outside that range, has been proposed and simulated. Also in Ref. [26], a channel add-drop filter is proposed as an application of the band stop filter, but, we have proposed and investigated a power splitter as an application of the band pass filter. The filter was proposed and investigated with silver metal or photonic crystal before[28,29] and here, we proposed it with graphene. The graphene-based structures have the most important advantage of conductivity tunability compared to the metallic- and photonic crystal-structures.[28,29] The graphene tunable conductivity gives the opportunity of altering the resonance characteristics without need for refabrication of the device. Our proposed planar graphene based filter has a minimum full width at half maximum (FWHM) of 110 nm (better than Refs. [30]– [35]) and a maximum transmission ratio of 0.7 (better than Refs. [36]– [39]) which are newly published as graphene-based filters. In addition, some other useful novel ultra-compact structures such as mode separator, multi/demultiplexer, switches, and logic gates and circuits could be proposed and designed based on the introduced

†Corresponding author. E-mail: granpayeh@kntu.ac.ir

© 2018 Chinese Physical Society and IOP Publishing Ltd

novel planar filter. The filter could be a useful functional structure in future nano devices and circuits. Graphene has some advantages compared to metals and photonic crystals, such as tunable conductivity, extreme confinement of plasmons, low losses, small size, and long propagation length.[6,7] So, graphene can be considered as a novel plasmonic material in the infrared region.[40] The proposed filter exhibits novel outstanding features and will be utilized in the construction of ultra-compact nano-scale devices and integrated circuits in the mid-infrared region for optical communications, processing, and computing.

The remainder of the paper is organized as follows. In Section 2, the device geometry and analysis method are described. In Section 3, the numerical results are given and discussed. The paper is concluded in Section 4.

2. Geometry, modeling, and method of analysis

The schematic view of the planar graphene based band-pass filter is shown in Fig. 1. It consists of two graphene ribbons as input/output ports and a graphene ring, as the resonator, between them. One end of each ribbon acts as the input or output port. The filter must be located on a dielectric medium such as Si_{O2}[41] or A_{l2O3}[42] for practical applications. For simplicity and without limiting the generality, we have assumed that the background of the filter is air in our FDTD simulations.

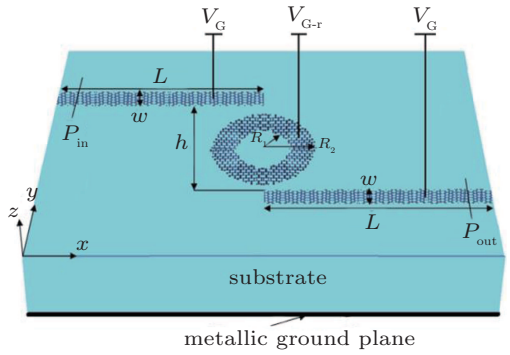


Fig. 1. (color online) Three-dimensional schematic view of our proposed graphene-based planar band-pass filter consisting of two graphene ribbons as input/output ports and a graphene ring between them as a resonator. The input/output ribbons have a gate voltage value of V_G, and the graphene ring resonator has a gate voltage value of $V_{G\text{-}r}$. The inner and the outer radii of the ring, the graphene ribbons width, the lengths of the input/output ribbons, the distance between the input/output ribbons, and the distance between the left end of the output ribbon and the center of the ring are R_1, R_2, W, L, h, and d, respectively. Two monitors at the points P_{in} and P_{out} measure the input and output optical powers. One dipole point source is placed 2 nm above the input ribbon to excite SPPs. Only the resonance wavelengths of the ring resonator transmit effectively to the output ribbon port. The structure should be located on a dielectric substrate. In our FDTD simulations, we assume the substrate is air.

In our simulations, the ultra-narrow graphene ribbon with a width of 10 nm[27,43–47] supports SPPs in the mid-infrared region. The surface conductivity (σ_g) of graphene is supported by Kubo's formula[48]

$$\sigma_g = \frac{i e^2 \mu_c}{\pi\hbar^2(\omega + i\tau^{-1})} + \frac{i e^2}{4\pi\hbar}\ln\left[\frac{2\mu_c - (\omega + i\tau^{-1})\hbar}{2\mu_c + (\omega + i\tau^{-1})\hbar}\right] + \frac{i e^2 k_B T}{\pi\hbar^2(\omega + i\tau^{-1})}\ln\left[\exp\left(-\frac{\mu_c}{k_B T}\right) + 1\right], \quad (1)$$

which depends on the momentum relaxation time, τ, temperature, T, chemical potential (Fermi energy), μ_c, and incident angular frequency, ω. The Kubo optical conductivity formula at room temperature simplifies to[49]

$$\sigma_g = \frac{i e^2 \mu_c}{\pi\hbar^2(\omega + i\tau^{-1})}, \quad (2)$$

which the intraband transition dominates, where the interband transition is neglected because the photon energy in the simulated wavelength range is always less than $2\mu_c$.[49] The carrier relaxation time is

$$\tau = \frac{\mu\mu_c}{e v_f^2}, \quad (3)$$

where μ and v_f are the carrier mobility and the Fermi velocity of graphene, respectively. In our simulations, the equivalent dielectric permittivity of graphene is calculated by[49]

$$\varepsilon_{eq} = 1 + i\frac{\sigma_g \eta_0}{k_0 \Delta}, \quad (4)$$

where Δ is the thickness of the graphene ribbon in the z direction and is assumed to be 1 nm. k_0 is the vacuum wavenumber and η_0 is the wave impedance of the air β_{SPP}, and the propagation constant of SPPs in the graphene ring is calculated by[49]

$$\beta_{SPP} = k_0 n_{eff} = k_0\sqrt{1 - \left(\frac{2}{\eta_0\sigma_g}\right)^2}, \quad (5)$$

where n_{eff} is the effective refractive index of SPPs in graphene. The theoretical resonance equation of the ring is[26]

$$\frac{J_n'(\beta_{SPP}R_2)}{J_n'(\beta_{SPP}R_1)} - \frac{N_n'(\beta_{SPP}R_2)}{N_n'(\beta_{SPP}R_1)} = 0, \quad (6)$$

where R_2 and $R_1 = R_2 - W$ are the outer and the inner radii of the graphene ring, respectively. J_n' and N_n' are the derivations of the Bessel functions of the first and the second kinds with order n, respectively. The first and second order resonance modes, modes 1 and 2, correspond to the first and second order Bessel and Hankel's functions, respectively.[26] The plasmon wavelength in graphene is given by[50]

$$\lambda_{sp} = \lambda_0\alpha\frac{4\mu_c}{\hbar(\varepsilon_r + 1)(\omega + i\tau^{-1})}, \quad (7)$$

where[47]

$$\alpha = \frac{e^2}{4\pi\varepsilon_0\hbar c} \approx \frac{1}{137}, \quad (8)$$

where ε_r is the permittivity of graphene.[49]

The structural parameters are chosen as $R_2 = 30$, and $W = 10$ nm. The material parameters related to the surface conductivity of graphene are assumed as follows: $\mu = 10^4$ cm^2/V·s,

$v_f = 10^6$ m/s, $\mu_c = 0.35$ eV. One dipole point source with transverse electric (TE) polarization, located 2 nm above the input graphene ribbon in the z direction, is used in our simulations to excite the SPP waves.[26,27] Two monitors are used to measure the input power, P_{in}, and the transmitted power, P_{out}. The transmittance (normalized transmission) spectrum is calculated by $T = P_{out}/P_{in}$.

3. Numerical results and discussion

In this section, the performances of planar filter and power splitter are proposed, analyzed, and discussed.

3.1. Planar filter

FDTD simulation results of the filter of Fig. 1 are illustrated in Fig. 2. In Figs. (2a) and (2b) the input and output transmittance spectra of the band-pass filter for the first and the second order resonance modes are shown. Two peaks corresponding respectively to the incident wavelengths of 6.1 μm ($\lambda_{SPP} = 44$ nm: Eqs. (7) and (8)) and 10.2 μm ($\lambda_{SPP} = 88$ nm: Eqs. (7) and (8)) appear in the transmittance spectrum and the prominent band-pass filtering effect is obtained in the mid-infrared region.

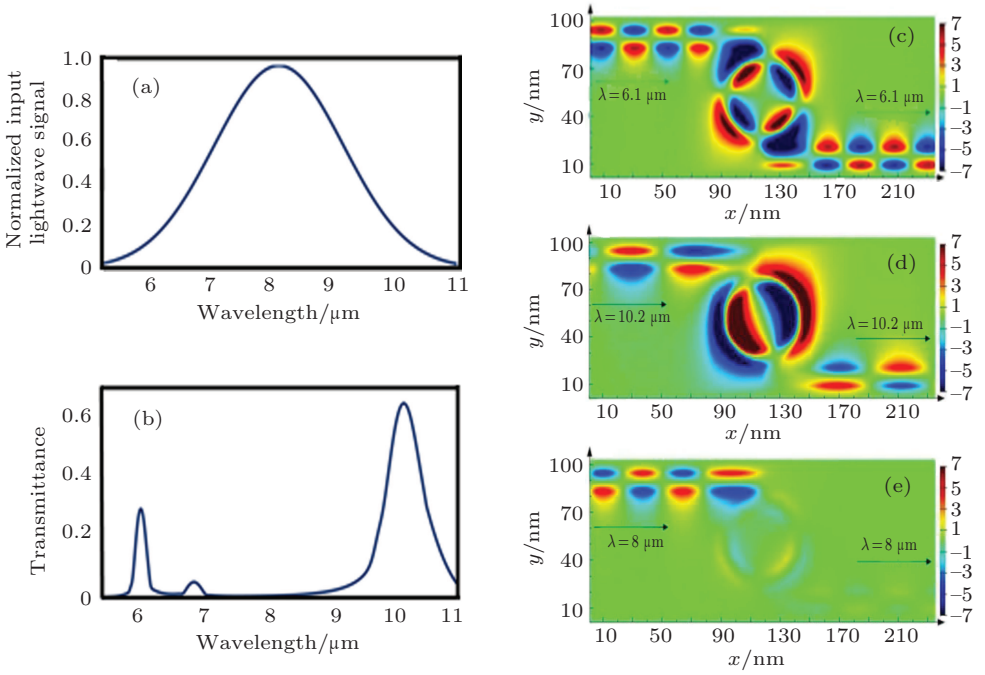


Fig. 2. (color online) (a) Normalized input lightwave signal and (b) the transmittance spectrum of the filter of Fig. 1. Distributions of the H_z fields in the xy cross section of the filter for three different wavelengths of (c) $\lambda = 6.1$ μm, (d) $\lambda = 10.2$ μm, resonant wavelengths, and (e) $\lambda = 8$ μm, non-resonant wavelength. Only the resonance wavelength of the ring transmits effectively to the output, which shows the filtering effect. Parameters of the ring are set as $R_2 = 30$ nm and $\mu_c = 0.35$ eV.

The structure is analyzed numerically by using the three-dimensional finite-difference time-domain (3D-FDTD) method with a 16-layer perfectly matched layer (PML) absorbing boundary condition around it. To reduce the computational time of our simulations, we have used a non-uniform mesh. In our simulations, the minimum mesh sizes inside the graphene are 0.1 nm and 1 nm in z and y directions, respectively. The minimum mesh sizes in the x direction of graphene ring and input/output ribbons are 1 nm and 1 nm, respectively. The mesh sizes increase gradually outside the graphene. Simulation parameters are given in Table 1.

Table 1. Simulation parameters and their values.

Parameter	Value	Parameter	Value
Graphene thickness in z direction (Δ)	1 nm	Number of PML layers	16
Graphene carrier mobility (μ)	10^4 cm^2/V·s	Minimum mesh size of graphene input/output ribbons in x direction	1 nm
Graphene Fermi velocity (v_f)	10^6 m/s	Minimum mesh size of graphene ring in x and y directions	1 nm
Minimum mesh size of graphene ring in z direction	0.1 nm	Chemical potential of input/output graphene ribbons	0.35 eV
Minimum mesh size of graphene input/output ribbons in y direction	1 nm	Velocity of light in vacuum (c)	3×10^8 m/s
Minimum mesh size of graphene input/output ribbons in z direction	0.1 nm	Distance between input/output graphene ribbons (h)	76 nm
Graphene ribbon width (W)	10 nm	Length of input/output graphene ribbons (L)	300 nm
The distance between the left end of the output ribbon and the center of the ring (d)	0 nm		

Distributions of the H_z fields in the xy cross section of the filter of Fig. 1 at the incident wavelengths of $\lambda = 6.1$ μm and $\lambda = 10.2$ μm are depicted in Figs. 2(c) and 2(d), respectively. The incident wavelengths of 6.1 μm and 10.2 μm, which satisfy the resonance condition, couple effectively to the ring resonator and finally decouple to the other graphene output ribbon, demonstrating the band-pass filtering effect.

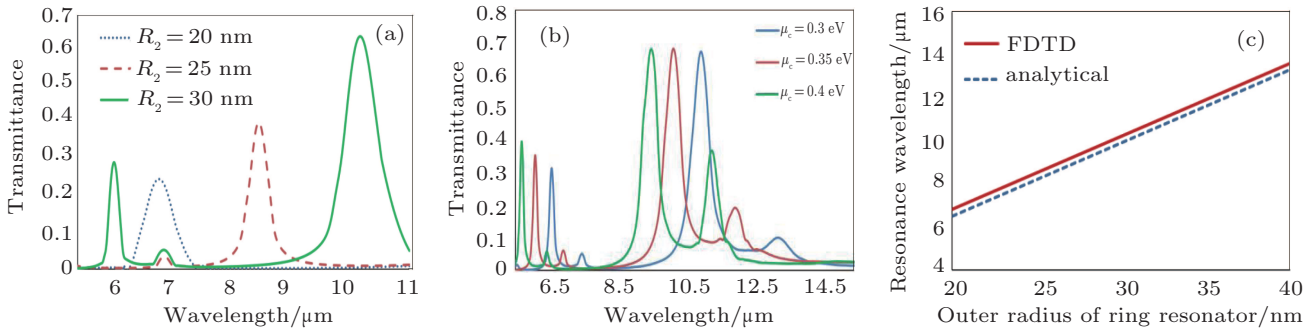


Fig. 3. (color online) Simulated transmittance spectra of the band-pass filter of Fig. 1 with (a) three different outer radii (R_2) of the graphene ring resonator with chemical potential of $\mu_c = 0.35$ eV, and (b) three different chemical potentials (μ_c) of the graphene ring with outer radius of 30 nm. (c) Comparisons of the resonance wavelengths of the first order mode of the graphene ring resonator versus its outer radius obtained by the FDTD method and the analytical resonance Eq. (6) of the ring resonator. The chemical potential of the ring is assumed to be $\mu_c = 0.35$ eV.

The radius of the graphene ring resonator affects the resonance wavelength of the structure, which is derived by the FDTD method and depicted in Fig. 3(a). In Fig. 3(a), transmittance spectra corresponding to the ring resonator with three different ring resonator radii are shown. As the radius of the ring increases, the resonance wavelength and the peak values increase which exhibit a red shift.[17,26] In Fig. 3(b), transmittance spectra of the ring resonator with three different chemical potentials are shown. As demonstrated, only the resonance wavelength of the ring resonator couples effectively to the output ribbon and the structure acts as a band-pass filter. As the chemical potential of the ring increases the resonance wavelength decreases, so the peak values increase, which exhibit a blue shift.[17,26] According to Eq. (2), variation of chemical potential, μ_c, changes the σ_g, so, by substituting Eqs. (2) and 6 in Eq. (5), the resonance wavelengths alter by changing μ_c, as shown in Fig. 3(b). As μ_c increases, transmission peaks increase, since the higher conductivity value results in a higher transmission peak value and SPP loss decreases. So, β_{SPP} increases and the resonance wavelength decreases. Also, we see that there is an indirect relationship between μ_c and the resonance wavelength (Eqs. (6), (7), and (8)). The transmission peaks exhibit a blue shift as the chemical potential increases. The analytical results of Eq. (6) are in good agreement with the FDTD simulation ones, as depicted in Fig. 3(c), where the first order resonance wavelengths of the transmittance versus outer radius of the graphene ring resonator are shown. It is possible to solve Eqs. (2), (3), (5), and (6) by using a MATLAB code to get Fig. 3(c). For this approach, first, by using Eq. (6), where R_1 and R_2 are known and $w = 10$ nm, we gain β_{SPP}. Then, τ and σ_g are calculated by using Eqs. (2) and (3). Finally, by using Eq. (5), k_0 and the resonance wavelengths can be obtained. Thus, the filter transmittance spectrum can be tuned by variation of the radius or the chemical potential of the ring resonator.

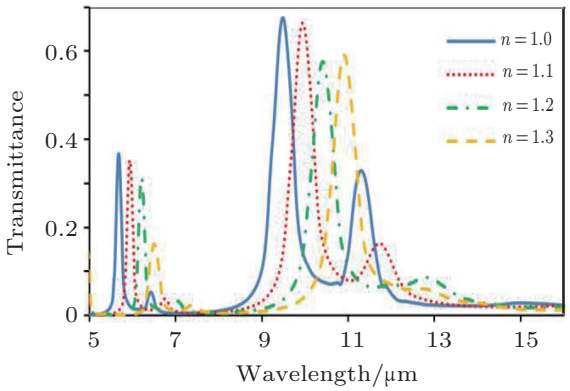


Fig. 4. (color online) Simulated transmittance spectra of the band-pass filter of Fig. 1 with four different dielectric substrate refractive indices with chemical potential of $\mu_c = 0.4$ eV and outer radius of $R_2 = 30$ nm.

By Eq. (6), we realize that there is a direct relationship between the ring resonance wavelength and its radius, and an indirect relationship between the resonance wavelengths and the chemical potential of the ring. If we locate the filter on a dielectric substrate, its refractive index affects the resonance wavelength of the ring, which is suitable for designing refractive index sensors. In theory, it should multiply the wavenumber of the graphene ring. Simulated transmittance spectra for four different substrates are given in Fig. 4. By variation of the distance between input/output graphene ribbons, h, the resonance wavelength will not change, because only the ring and its parameters such as its radius and its chemical potential affect the resonance wavelength of the resonator, as it is clear in Eqs. (2), (3), (5), and (6), but the resonance peak values decrease. By increasing this distance, coupling between the input/output ports and the ring decreases. The simulated transmittance spectra for three different h are illustrated in Fig. 5.

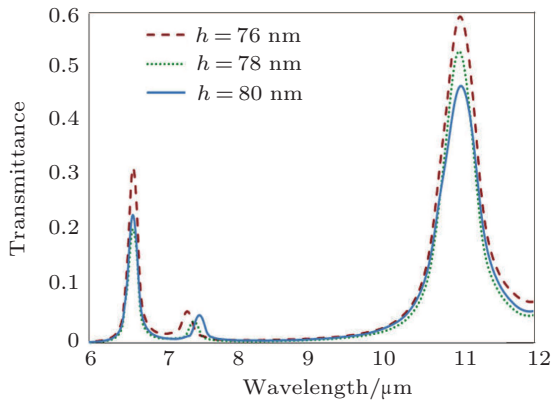


Fig. 5. (color online) Simulated transmittance spectra of the band-pass filter of Fig. 1 with three different distances between input/output ribbons (h) with chemical potential of $\mu_c = 0.3$ eV and outer radius of $R_2 = 30$ nm.

If $d \neq 0$, Fano resonance, the coupling of two resonances of different damping rates, produces the narrow and broad spectral lines. The final spectrum is a sum of these two resonances giving the characteristic asymmetry of the Fano resonance peak. This will occur at the left side of the transmittance spectra. For a metallic ring resonator, Fano resonance and refractive index sensing was investigated and analyzed carefully in Ref. [51]. Fano resonance and refractive index sensing could also be analyzed and investigated for the graphene-based planar filter.

Table 2. Minimum FWHM in some work.

Ref.	Minimum FWHM/nm
[30]	300
[31]	400
[32]	140
[33]	237
[34]	42
[35]	20
This work	110

Table 3. Maximum transmission ratio in some work.

Ref.	Maximum transmission ratio
[36]	0.5
[37]	0.4
[38]	0.38
[39]	0.25
This work	0.7

The minimum full width at half maximum (FWHM) for the first and second order resonance wavelengths are 480 nm and 110 nm, respectively. The minimum FWHMs in some graphene-based structures are given in Table 2. The FWHM of our proposed filter is improved compared to them; however, some articles reached lower FWHMs. The maximum transmission ratios in some graphene-based structures are given in Table 3. In our proposed planar filter, the maximum transmission ratio reaches to 0.7. Our proposed planar filter is a useful structure in the mid infrared wavelength range.

Also, compared to metallic ring filters,[28,29] our proposed graphene based filter has smaller size and tunable conductivity, which makes it a useful wavelength selective structure.

3.2. Power splitter

One of the applications of the filter of Fig. 1 is a power splitter. The three dimensional schematic view of the power splitter is depicted in Fig. 6. It is composed of an input graphene ribbon, a ring resonator, and two output graphene ribbons. All the simulation parameters are the same as those in Fig. 2(d) and L' are assumed to be 12 nm and 268 nm, respectively. Transmittance spectra and distributions of the H_z fields in the xy cross section of the power splitter of Fig. 6 at the incident wavelengths of $\lambda = 6.1$ μm and $\lambda = 10.2$ μm are demonstrated in Figs. 7(a)–7(c).

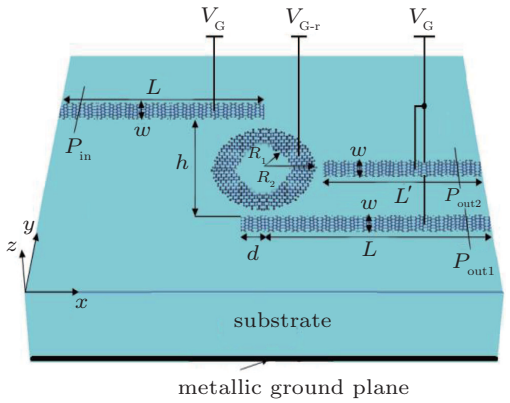


Fig. 6. (color online) (a) Three-dimensional schematic view of our proposed graphene based power splitter. d and L' are assumed to be 12 nm and 268 nm, respectively. Other simulation parameters are the same as those in Fig. 2.

As illustrated in the field distributions of Figs. 7(b) and 7(c), the second order resonance mode splits equally between output ports, but the first order resonance mode couples effectively to output port 1. We can verify our simulation results by the following analytical discussion, which can also be used for designing optical graphene based logic gates and circuits such as XOR, XNOR, and NOT. The incident magnetic field for the ring resonator with an average radius of $R = (R_1 + R_2)/2$ can be written as[52]

$$H^i = \hat{a}_z a^i \, \mathrm{e}^{-\mathrm{j}\beta_{\mathrm{spp}} x} = \hat{a}_z \sum_{n=-\infty}^{\infty} a_n^i \, \mathrm{j}^{-n} \, \mathrm{J}_n \left(\beta_{\mathrm{spp}} R\right) \mathrm{e}^{\mathrm{j}n\varphi}, \quad (9)$$

where φ and n denote the azimuth angle and the resonance mode order, respectively. The transmitted magnetic field to the ring resonator will be[52]

$$H^t = \hat{a}_z a^t \, \mathrm{e}^{-\mathrm{j}\beta_{\mathrm{spp}} x} = \hat{a}_z \sum_{n=-\infty}^{\infty} a_n^t \, \mathrm{j}^{-n} \, \mathrm{J}_n \left(\beta_{\mathrm{spp}} R\right) \mathrm{e}^{\mathrm{j}n\varphi}. \quad (10)$$

In the y direction, $\varphi = \pm\pi/2$ for the first-order resonance mode ($n = 1$), and by considering the relation between Bessel functions[52]

$$\mathrm{J}_{-n}(R) = (-1)^n \, \mathrm{J}_n(R), \quad (11)$$

we can find[50]

$$H^t_{n=1}\left(R, \varphi = \pm\frac{\pi}{2}\right) = 0. \tag{12}$$

So, the first order resonance mode cannot propagate in output port 2 (Fig. 7(c)). For the second order resonance mode ($n = 2$), we can find that

$$H^t_{n=2}\left(R, \varphi = \pm\frac{\pi}{2}\right) \neq 0. \tag{13}$$

So, the second order resonance mode can propagate in output port2 and its power splits equally between the two output ports (Fig. 7(b)).

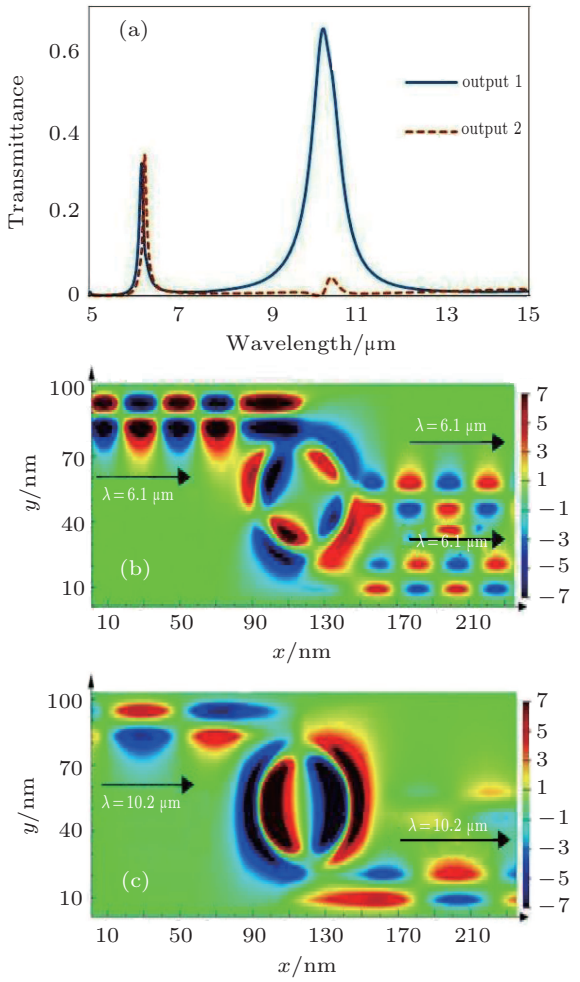


Fig. 7. (color online) (a) Output transmittance spectra of the power splitter of Fig. 7. Distributions of the H_z fields in the xy cross section of the power splitter for resonance wavelengths of (b) $\lambda = 6.1$ μm and (c) $\lambda = 10.2$ μm. d and L' are assumed to be 12 nm and 268 nm, respectively. Other simulation parameters are the same as those in Fig. 2.

The proposed planar filter will find many further applications in the design of some novel nano-scale devices such as plasmonic multi/demultiplexers,[53] channel add-drop filters,[16] switches with nonlinear Kerr self-phase modulation (SPM) and cross-phase modulation (XPM) effects,[54–56] sensors,[57,58] logic gates,[59] analog-to-digital converters,[60] decoders,[61] n-coders,[62] flip-flops,[63] delay lines,[64] plasmonically-induced transparency (PIT), and perfect absorptions[65–67] in photonic integrated circuits. The noticeable advantage of these graphene-based devices is that the performance wavelength of them can be tuned easily by applying bias voltage to the graphene waveguides and ring resonators.

4. Conclusion

In this paper, the performance of a graphene band-pass filter is proposed and investigated theoretically and numerically by using the three-dimensional finite-difference time-domain (3D-FDTD) method. The proposed structure works in the mid-infrared wavelength region. The ring resonance wavelengths can be changed by variation of the radius of the graphene ring resonator, the dielectric substrate of the device or by variation of the gate voltage of the graphene ring resonator to change the graphene chemical potential (Fermi energy). The FDTD simulation results are in good agreement with the theoretical calculation ones. For an application of our filter, a power splitter is designed and simulated. Therefore, the proposed filter will find utility in the design of the ultra-compact, nano-scale devices such as optical multi/demultiplexers, channel add-drop filters, switches, sensors, logic gates, logic circuits, and delay lines in photonic integrated circuits.

References

[1] Barnes W L, Dereux A and Ebbesen T W 2003 *Nature* **424** 824
[2] Wang G, Lu H and Liu X 2012 *Appl. Phys. Lett.* **101** 013111
[3] Gómez-Santos G and Stauber T 2012 *Europhys. Lett.* **99** 27006
[4] Wang Y, Wang J, Gao S and Liu C 2013 *Appl. Phys. Express* **6** 022003
[5] Moghadasi M N, Zarrabi F B, Pandesh S, Rajabloo H and Bazgir M 2016 *Opt. Quantum Electron.* **48** 266
[6] Bonaccorso F, Sun Z, Hasan T and Ferrari A C 2010 *Nat. Photon.* **4** 611
[7] García de Abajo F J 2014 *ACS Photon.* **1** 135
[8] Li P and Taubner T 2012 *ACS Nano* **6** 10107
[9] Wu H Q, Linghu C Y, Lu H M and Qian H 2013 *Chin. Phys. B* **22** 098106
[10] Xu D G, Wang Y Y, Yu H, Li J Q, Li Z X, Yan C, Zhang H, Liu P X, Zhong K and Wang W P 2014 *Chin Phys. B* **23** 054210
[11] Liu Z K, Xie Y N, Geng L, Pan D K and Song P 2016 *Chin. Phys. Lett.* **33** 027802
[12] Sun J, Zhang L and Gao F 2016 *Chin. Phys. B* **25** 108701
[13] Jamalpoor K, Zarifkar A and Miri M 2017 *Photonics Nanostruct.-Fundam. Appl.* **26** 80
[14] Huang B H, Lu W B, Li X B, Wang J and Liu Z G 2016 *Appl. Opt.* **55** 5598
[15] Ghahri M R and Faez R 2017 *Appl. Opt.* **56** 4926
[16] Asgari S and Granpayeh N 2017 *J. Nanophoton.* **11** 026012
[17] Asgari S, Dolatabady A and Granpayeh N 2017 *Opt. Eng.* **56** 067102
[18] Zhang Y P, Li T T, Lv H H, Huang X Y, Zhang X, Xu S L and Zhang H Y 2015 *Chin. Phys. Lett.* **32** 068101
[19] Wang Z, Deng Y and Sun L F 2017 *Chin. Phys. B* **26** 114101
[20] Yan B, Yang X X, Fang J Y, Huang Y D, Qin H and Qin S Q 2014 *Chin. Phys. B* **24** 015203
[21] Nikitin Y, Guinea F, Garcia-Vidal F J and Martin-Moreno L 2011 *Phys. Rev. B* **84** 161407
[22] Nikitin A Y, Guinea F, Garcia-Vidal F J and Martin-Moreno L 2012 *Phys. Rev. B* **85** 081405

[23] Fei Z, Goldflam M D, Wu J S, Dai S, Wagner M, Mcleod A S, Liu M K, Post K W, Zhu S, Janssen G C A M, Fogler M M and Basov D N 2015 *Nano Lett.* 5b03834

[24] Zhuang H, Kong F, Li K and Sheng S 2015 *Appl. Opt.* **54** 7455

[25] Sheng S, Li K, Kong F and Zhuang H 2015 *Opt. Commun.* **336** 189

[26] Li H J, Wang L L, Liu J Q, Huang Z R, Sun B and Zhai X 2013 *Appl. Phys. Lett.* **103** 211104

[27] Han X, Wang T, Li X, Xiao S and Zhu Y 2015 *Opt. Express* **23** 31945

[28] Zou S Wang F, Liang R, Xiao L and Hu M 2015 *IEEE Sens. J.* **15** 646

[29] Chen Y, Wang W Y and Zhu Q 2014 *Optik* **125** 3931

[30] Li H J, Wang L L and Zhai X 2016 *Sci. Rep.* **6** 36651

[31] Goldflam M D, Fei Z, Ruiz I, Howell S W, Davids P S, Peters D W and Beechem T E 2017 *Opt. Express* **25** 12400

[32] Meng H, Wang L, Liu G, Xue X, Lin Q and Zhai X 2017 *Appl. Opt.* **56** 6022

[33] Li H J, Wang L L, Sun B, Huang Z R and Zhai X 2014 *Appl. Phys. Express* **7** 125101

[34] Li H J, Wang L L, Zhang H, Huang Z R, Sun B, Zhai X and Wen S C 2014 *Appl. Phys. Express* **7** 024301

[35] Guo C C, Zhu Z H, Yuan X D, Ye W M, Liu K, Zhang J F, Xu W and Qin S Q 2016 *Adv. Opt. Mater.* **4** 1955

[36] Asgari S and Granpayeh N 2017 *Opt. Commun.* **393** 5

[37] He M D, Wang K J, Wang L, Li J B, Liu J Q, Huang Z R, Wang L L, Wang L, Hu W D and Chen X 2014 *Appl. Phys. Lett.* **105** 081903

[38] Li H J, Wang L L, Huang Z R, Sun B and Zhai X 2015 *Plasmonics* **10** 39

[39] Li H J, Wang L L, Sun B, Huang Z R and Zhai X 2014 *Appl. Phys. Express* **7** 125101

[40] Christensen J, Manjavacas A, Thongrattanasiri S, Koppens F H L and García de Abajo F J 2012 *ACS Nano* **6** 431

[41] Chen J, Badioli M, Gonzalez P A, Thongrattanasiri S, Huth F, Osmond J, Spasenovic M, Centeno A, Pesquera A, Godignon P, Elorza A Z, Camara N, Abajo F J G D, Hillenbrand R and Koppens F H L 2012 *Nature* **487** 77

[42] Min B K, Kim S K, Kim S J, Kim S H, Kang M A, Park C Y, Song W, Myung S, Lim J and An K S 2015 *Sci. Rep.* **5** 16001

[43] Li H J, Wang L L, Liu J Q, Huang Z R, Sun B and Zhai X 2014 *Plasmonics* **9** 1239

[44] Li H J, Wang L L, Sun B, Huang Z R and Zhai X 2016 *Plasmonics* **11** 87

[45] Li H J, Wang L L, Zhang B H and Zhai X 2016 *Appl. Phys. Express.* **9** 012001

[46] Yan X, Wang T, Han X, Xiao S, Zhu Y and Wang Y 2017 *Plasmonics* **12** 1449

[47] Celis A, Nair M N, Taleb-Ibrahimi A, Conrad E H, Berger C, de Heer W A and Tejeda A 2016 *J. Phys. D: Appl. Phys.* **49** 143001

[48] Lin H, Pantoja M F, Angulo L D, Alvarez J, Martin R G and Garcia S G 2012 *IEEE Mic. Wire. Comp. Lett.* **22** 612

[49] Wang B, Zhang X, Yuan X and Teng J 2012 *Appl. Phys. Lett.* **100** 131111

[50] Luo X, Teng Q, Weibing L and Zhenhua N 2013 *Mater. Sci. Eng. R: Reports* **74** 351

[51] Yan S B, Luo L, Xue C Y and Zhang Z D 2015 *Sensors* **15** 29183

[52] Balanis C 2012 *Advanced Engineering Electromagnetics*, 2nd. edn., Chap. 11 (Wiley, USA)

[53] Nurmohammadi T, Abbasian K and Yadipoura R 2017 *Optik* **142** 550

[54] He Z, Li H, Zhan, Li B, Chen Z and Xu H 2015 *Sci. Rep.* **5** 15837

[55] Nurmohammadia T, Abbasian K and Yadipoura R 2018 *Opt. Commun.* **410** 142

[56] Nozhat N and Granpayeh N 2014 *J. Mod. Opt.* **61** 1690

[57] Zhang Z, Yang J, He X, Zhang J, Huang J, Chen D and Han Y 2018 *Sensors* **18** 1

[58] Kwon S H 2017 *Sensors* **17** 11

[59] Nozhat N and Granpayeh N 2015 *Appl. Opt.* **54** 7944

[60] Mehdizadeh F, Soroosh M, Banaei H A and Farshidi E 2017 *Appl. Opt.* **56** 1799

[61] Daghooghi T, Soroosh M and Ansari-Asl K 2018 *Appl. Opt.* **57** 2250

[62] Ouahab I and Naoum R 2016 *J. Optik* **127** 7835

[63] Moniem T A 2015 *Opt. Quantum Electron.* **47** 2843

[64] Lu Q, Liu Q, Jiang W, Xia J and Huang Q 2017 *IEEE Photon. J.* **9** 4900611

[65] Xia S X, Zhai X, Wang L L, Sun B, Liu J Q and Wen S C 2016 *Opt. Express* **24** 17886

[66] Xia S X, Zhai X, Huang Y, Liu J Q, Wang L L and Wen S C 2017 *J. Lightw. Technol.* **35** 4553

[67] Xia S X, Zhai X, Huang Y, Liu J Q, Wang L L and Wen S C 2017 *Opt. Lett.* **42** 3052